The Method of Small Volume Expansions for Emerging Medical Imaging

Habib Ammari

CNRS & Ecole Polytechnique

Motivation and Principles of the MSVE

- Inverse problems in medical imaging: ill-posed, they literally have no solution! (Steven Pinker, *How the Minds Work ?*)

(a) MRI Image of breast cancer

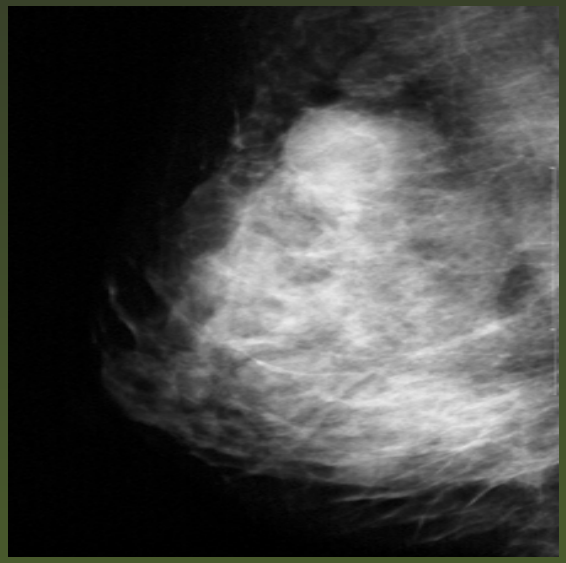

(b) X-ray image of breast cancer

Motivation and Principles of the MSVE

- Multi-physics Imaging Methods.
- Multi-scale Imaging Methods: Add structural information or supply missing information (kind of regularization) to determine specific features with satisfactory resolution. One such knowledge: find unknown small anomalies (potential tumors at early stage)
- MSVE key role
- Emerging Medical applications: electrical impedance tomography (EIT), radiation force imaging, impediography (EIT by Ultrasound Focusing), magnetic resonance elastography, and photo-acoustic imaging.

Emerging Medical Applications

- EIT: impose boundary voltages, measure the induced boundary currents to estimate the electrical conductivity.
- Radiation force imaging: generate vibrations inside the organ, acquire a spatio-temporal sequence of the propagation of the induced transient wave inside the organ to estimate its viscoelastic parameters.
- Impediography: use an EIT system, perturb the medium during the electric measurements, by focusing ultrasonic waves on regions of small diameter inside the organ $\rightarrow$ the pointwise value of the electrical energy density at the center of the perturbed zone. Find the conductivity distribution. (Patent WO 2008/037929 A2).

Emerging Medical Applications

- Magnetic resonance elastography: reconstruct the shear modulus from measurements of the displacement field in the whole organ.
- Photo-acoustic imaging: generation of acoustic waves by the absorption of optical energy. Reconstruct absorbing regions inside the organ from boundary measurements of the induced acoustic signal.

Principles of the Imaging Techniques

- Boundary and Scattering Measurements: EIT
  - anomaly detection
- Internal Measurements: Radiation force imaging, MRE
  - distribution of physical parameters
- Boundary Measurements from Internal Perturbations of the Medium: Impediography, photo-acoustic imaging.
  - distribution of physical parameters

Motivation and Principles of the MSVE

Small volume asymptotic expansions:

- Boundary Measurements: outer expansions in terms of the characteristic size of the anomaly
  - anomaly detection
- Internal Measurements: inner expansions
  - distribution of physical parameters

Reference

- *An Introduction to Mathematics of Emerging Biomedical Imaging, Mathématiques & Applications, Vol. 62, Springer, Berlin, 2008.*

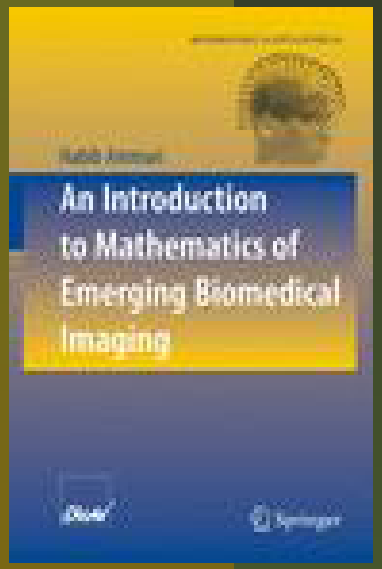

Conductivity Problem

Notation: $\Omega \in \mathbb{R}^d (d \geq 2)$: smooth bounded domain.
$N(x,z)$: Neumann function for $-\Delta$ in Ω corresponding to a Dirac mass at $z \in \Omega$:

$$\begin{cases} -\Delta_x N(x,z) = \delta_z \quad \text{in } \Omega \ , \\ \dfrac{\partial N}{\partial \nu_x}\Big|_{\partial\Omega} = -\dfrac{1}{|\partial\Omega|} \ , \displaystyle\int_{\partial\Omega} N(x,z)\, d\sigma(x) = 0 \ . \end{cases}$$

B: smooth bounded domain. $\hat{v}$: corrector the solution to

$$\begin{cases} \Delta\hat{v} = 0 \quad \text{in } \mathbb{R}^d \setminus \overline{B} \ , \quad \Delta\hat{v} = 0 \quad \text{in } B \ , \\ \hat{v}|_- - \hat{v}|_+ = 0 \quad \text{on } \partial B \ , \quad k\dfrac{\partial\hat{v}}{\partial\nu}|_- - \dfrac{\partial\hat{v}}{\partial\nu}|_+ = 0 \quad \text{on } \partial B \ , \\ \hat{v}(\xi) - \xi \to 0 \quad \text{as } |\xi| \to +\infty \ . \end{cases}$$

Conductivity Problem

$D = \delta B + z$: anomaly $\subset \Omega$; δ: characteristic size of the anomaly; conductivity $0 < k \neq 1 < +\infty$.

The voltage potential u:

$$\begin{cases} \nabla \cdot \Big(\chi(\Omega \setminus \overline{D}) + k\chi(D) \Big) \nabla u = 0 \quad \text{in } \Omega \ , \\ \left. \dfrac{\partial u}{\partial \nu} \right|_{\partial\Omega} = g \quad \left(g \in L^2(\partial\Omega), \displaystyle\int_{\partial\Omega} g \, d\sigma = 0 \right) \ , \\ \displaystyle\int_{\partial\Omega} u \, d\sigma = 0 \ . \end{cases}$$

U: the background solution.

Outer Expansion

- A. Friedman, M. Vogelius, J.K. Seo, H. Kang, . . .
- Dipole-type approximation of the conductivity anomaly.
- The following boundary asymptotic (outer) expansion on $\partial\Omega$ holds for $d = 2, 3$:

$$(u - U)(x) \approx -\delta^d \nabla U(z) M(k, B) \nabla_z N(x, z) \ .$$

- $M(k, B) := (k - 1) \int_B \nabla \hat{v}(\xi) \, d\xi$: the polarization tensor (PT)
- The location z and the matrix $M(k, B)$: reconstructed.
- $M(k, B)$: characterizes all the information about the anomaly that can be learned from boundary measurements.
- $M(k, B)$: mixture of k and low-frequency geometric information.

Polarization Tensor

- Properties of the polarization tensor:

  (i) M is symmetric.

  (ii) If $k > 1$, then M is positive definite, and it is negative definite if $0 < k < 1$.

  (iii) Hashin-Shtrikman bounds:

$$\begin{cases} \dfrac{1}{k-1}\,\mathrm{trace}(M) \leq (d-1+\dfrac{1}{k})|B|\,, \\ (k-1)\,\mathrm{trace}(M^{-1}) \leq \dfrac{d-1+k}{|B|}\,. \end{cases}$$

- Optimal size estimates; Thickness estimates; Pólya–Szegö conjecture.

- Lipton, Capdeboscq-Vogelius, Capdeboscq-Kang, Kang-Milton.

Polarization Tensor

Visualization of PT

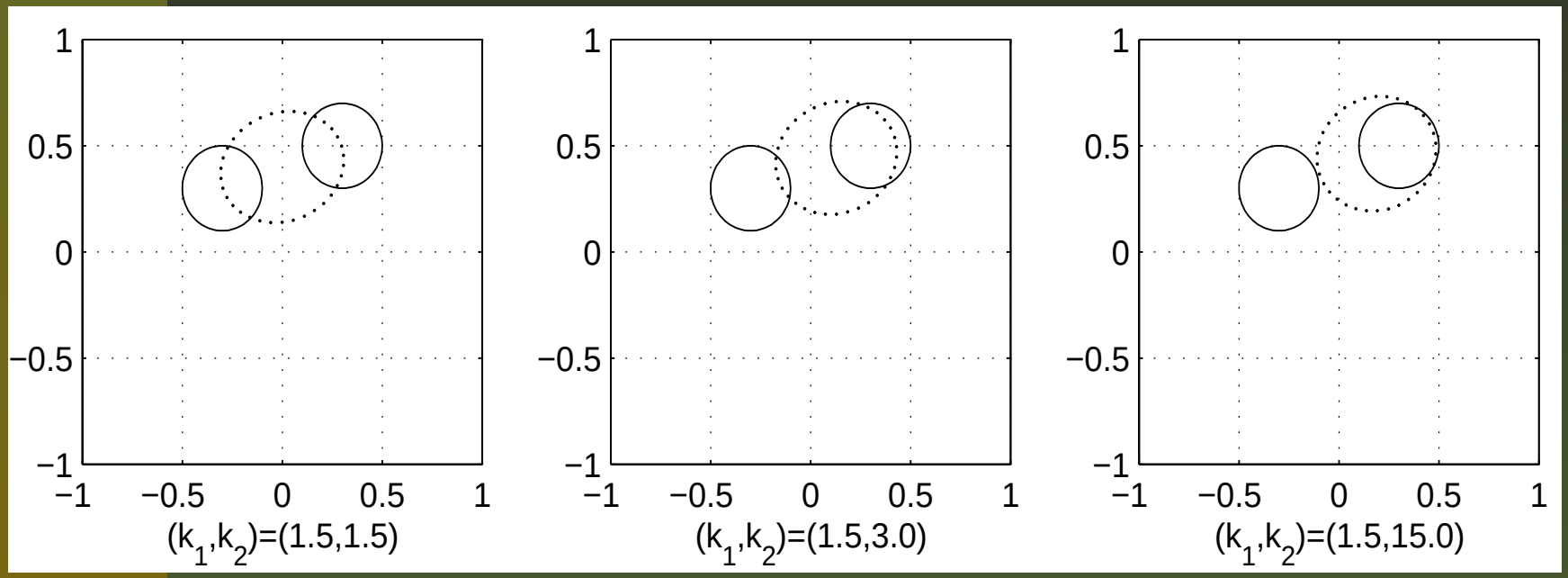

Figure 1: When the two disks have the same radius and the conductivity of the one on the right-hand side is increasing, the equivalent ellipse is moving toward the right anomaly.

Polarization Tensor

Visualization of PT

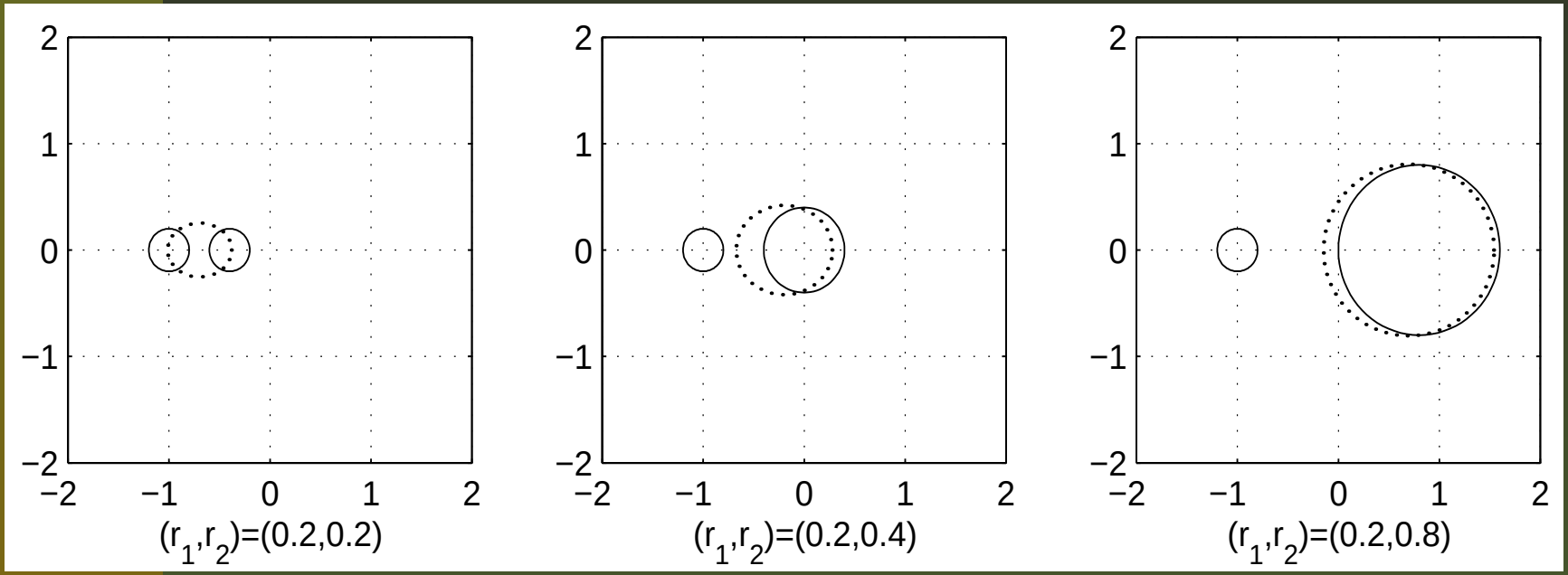

Figure 2: When the conductivities of the two disks is the same and the radius of the disk on the right-hand side is increasing, the equivalent ellipse is moving toward the right anomaly.

Polarization Tensor

- with H. Kang, *Polarization and Moment Tensors: With Applications in Imaging and Effective Medium Theory, Applied Mathematical Sciences, Vol. 162, Springer, New York, 2007.*

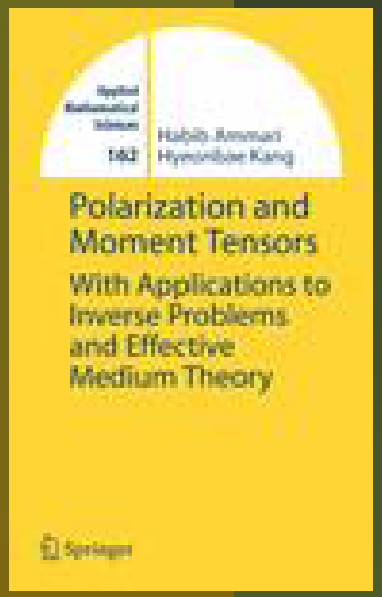

EIT Anomaly Detection System

- (with J.K. Seo, O. Kwon, and E.J. Woo, SIAP 05)
- EIT system for anomaly detection: location of the anomaly and reconstruction of its polarization tensor.
- Reconstruction depends on the boundary: inaccurate model of the boundary causes severe errors for the reconstructions
- Separate conductivity/size: Higher-order polarization tensors.
- Separate conductivity/size: Requires very sensitive EIT system.

Inner Expansion

The following inner asymptotic formula holds:

$$u(x) \approx U(z) + \delta \hat{v}(\frac{x-z}{\delta}) \cdot \nabla U(z) \quad \text{for } x \text{ near } z \ .$$

- Boundary independent reconstruction: no need of an exact knowledge of the boundary of the domain Ω
- Local Reconstruction
- Separate conductivity/ Geometry
- Interface Approximation: high frequency information

Acoustic Radiation Force

- (with P. Garapon, L. Guadarrama Bustos, and H. Kang, JDE 09)
- Use of the acoustic radiation force of an ultrasonic focused beam to remotely generate mechanical vibrations in organs.
- The radiation force acts as a dipolar source at the pushing ultrasonic beam focus.
- Generate the Green function of the medium.
- A spatio-temporal of the propagation of the induced transient wave can be acquired $\Rightarrow$ Quantitative estimation of the viscoelastic parameters of the studied medium in a source-free region.

Acoustic Radiation Force

- $U_y(x,t)$ retarded Green's function generated at $y \in \Omega$ and $t = 0$ without the anomaly.
- The wave in the presence of the anomaly:

$$\begin{cases} \partial_t^2 u - \nabla \cdot \big(\chi(\mathbb{R}^3 \setminus \overline{D}) + k\chi(D)\big)\nabla u = \delta_{x=y}\delta_{t=0}, \mathbb{R}^3 \times]0, +\infty[, \\ u(x,t) = 0 \quad \text{for} \quad x \in \mathbb{R}^3 \quad \text{and } t \ll 0. \end{cases}$$

- No (uniform) asymptotic formula for both high and low-frequencies.
- Truncate the high-frequency component of the signal up to $\rho = O(\delta^{-\alpha}), \alpha < \frac{1}{2}$,

$$P_\rho[u](x,t) = \int_{|\omega| \leq \rho} e^{-\sqrt{-1}\omega t} \hat{u}(x,\omega) d\omega.$$

Acoustic Radiation Force

- $T = |y - z|$ travel time between the source and the anomaly.
- After truncation of the high frequency component, the perturbation due to the anomaly is (approximately) a wave emitted from the point z at $t = T$.
- Truncation parameter ρ up to $O(\delta^{-\alpha}), \alpha < \frac{1}{2}$.
- Far field expansion of $P_\rho[u - U_y](x,t)$:

$$= -\delta^3 \int_{\mathbb{R}} \nabla P_\rho[U_z](x, t-\tau) \cdot M(k,B) \nabla P_\rho[U_y](z,\tau)\, d\tau$$
$$+ O(\epsilon^{4(1-\frac{3}{4}\alpha)}).$$

- The anomaly behaves then like a dipolar source.

Time-Reversal Imaging

- To detect the anomaly from far-field measurements one can use a time-reversal technique.
- One measures the perturbation on a closed surface surrounding the anomaly, truncates its high-frequency component, and retransmits it through the background medium in a time-reversed chronology.
- The perturbation will travel back to the location of the anomaly.

Time-Reversal Imaging

- The reversed wave (after high-frequency truncation)

$$w_{\text{tr}}(x,t) = \int_{\mathbb{R}} ds \int_S \Big[U_x(x',t-s) \frac{\partial P_\rho[u-U_y]}{\partial \nu}(x',t_0-s) - \frac{\partial U_x}{\partial \nu}(x',t-s) P_\rho[u-U_y](x',t_0-s) \Big] \, d\sigma(x').$$

- ($p := M(k,B)\nabla P_\rho[U_y](z,T)$)

$$w_{\text{tr}}(x,t) \approx -\epsilon^3 p \cdot \nabla_z \big[P_\rho[U_z](x,t_0-T-t) - P_\rho[U_z](x,t-t_0+T) \big].$$

- The reversed wave is the sum of incoming and outgoing spherical waves.

Time-Reversal Imaging

- Frequency domain (Φ_ω outgoing Green's function):

$$\int_S \left[\Phi_\omega(x-x') \overline{\frac{\partial \Phi_\omega}{\partial \nu}(z-x')} - \overline{\Phi_\omega}(z-x') \frac{\partial \Phi_\omega}{\partial \nu}(x-x') \right] d\sigma(x')$$

$$= 2\sqrt{-1}\Im m\, \Phi_\omega(z-x) \text{ (resolution limit in imaging).}$$

- Inhomogeneous media: similar formula.
- Resolution limit in imaging: size of the focal spot of order half the wavelength.
- Sharper the behavior of $\Im m\, \Phi_\omega$ at z, higher the resolution.
- Super-resolution: how the behavior of $\Im m\, \Phi_\omega$ depends on the heterogeneity of the medium ?

Imaging from Near-Field Measurements

- Near field expansion:

$$P_\rho[u - U_y](x,t) = \delta \hat{v}\left(\frac{x-z}{\delta}\right) \cdot \nabla P_\rho[U_y](x,t) + O(\delta^{2(1-\alpha)}).$$

- Local and accurate reconstruction from near field measurements.

Multi-Scale Approaches

- Far-field measurements: detection

$$(u-U)(x) \approx -(k-1)\delta^d \nabla U(z) \left(\int_B \nabla \hat{v}(\xi)\, d\xi \right) \nabla_z N(x,z)\ .$$

- Near-field measurements: shape reconstruction and material parameter characterization

$$u(x) \approx U(z) + \delta \hat{v}(\frac{x-z}{\delta}) \cdot \nabla U(z)\ .$$

Multi-Physics Approaches

- Impediography
- Magnetic resonance elastography
- Photo-acoustic imaging

Impediography

- (with E. Bonnetier, Y. Capdeboscq, M. Tanter, and M. Fink, SIAP 08)
- To couple electric measurements to localized acoustic perturbations.
- u the voltage potential induced by a current g, in the absence of acoustic perturbations:

$$\begin{cases} \nabla_x \cdot (\gamma(x)\nabla_x u) = 0 \text{ in } \Omega \ , \\ \gamma(x)\dfrac{\partial u}{\partial \nu} = g \text{ on } \partial\Omega \ , \end{cases}$$

Impediography

u_δ induced by g, in the presence of acoustic perturbations localized in a disk-shaped domain $D := z + \delta B$:

$$\begin{cases} \nabla_x \cdot (\gamma_\delta(x) \nabla_x u_\delta(x)) = 0 \text{ in } \Omega \ , \\ \gamma(x) \dfrac{\partial u_\delta}{\partial \nu} = g \text{ on } \partial\Omega \ , \end{cases}$$

$$\gamma_\delta(x) \ = \ \gamma(x) \Big[1 + \chi(D)(x) \, (\nu(x) - 1) \Big] \ .$$

$$\begin{aligned} \mathcal{E}(z) \ &= \ \left(\int_D \frac{(\nu(x) - 1)^2}{\nu(x) + 1} dx \right)^{-1} \int_{\partial\Omega} (u_\delta - u) g \, d\sigma \\ &\approx \ \gamma(z) \, |\nabla u(z)|^2 \end{aligned}$$

Impediography

- Inverse problem: reconstruct γ knowing $\mathcal{E} \approx \gamma \left|\nabla u\right|^2$ (electrical energy density).
- Substitute γ by $\mathcal{E} / \left|\nabla u\right|^2$.
- Nonlinear PDE (the 0–Laplacian)

$$\begin{cases} \nabla_x \cdot \left(\dfrac{\mathcal{E}}{\left|\nabla u\right|^2} \nabla u \right) = 0 \quad \text{in } \Omega \,, \\ \dfrac{\mathcal{E}}{\left|\nabla u\right|^2} \dfrac{\partial u}{\partial \nu} = g \quad \text{on } \partial\Omega \,. \end{cases}$$

- Choose two currents g_1 and g_2 s.t. $\nabla u_1 \times \nabla u_2 \neq 0$ for all $x \in \Omega$.
- The reconstruction algorithm is based on an approximation of a linearized version of the nonlinear 0–Laplacian problem.

Impediography

- Start from an initial guess for the conductivity γ, and solve the corresponding Dirichlet conductivity problem

$$\begin{cases} \nabla \cdot (\gamma \nabla u_0) = 0 & \text{in } \Omega \ , \\ u_0 = \psi & \text{on } \partial\Omega \ . \end{cases}$$

  ψ: the Dirichlet data measured as a response to the current g (say $g = g_1$) in absence of elastic deformation.

- The discrepancy between the data and the guessed solution:

$$\epsilon_0 := \frac{\mathcal{E}}{|\nabla u_0|^2} - \gamma \ .$$

Impediography

- Introduce a corrector:

$$\begin{cases} \nabla \cdot (\gamma \nabla \delta u) = -\nabla \cdot (\varepsilon_0 \nabla u_0) & \text{in } \Omega \ , \\ \delta u = 0 & \text{on } \partial\Omega \ , \end{cases}$$

- Update the conductivity

$$\gamma := \frac{\mathcal{E} - 2\gamma \nabla \delta u \cdot \nabla u_0}{|\nabla u_0|^2} \ .$$

- Iteratively update the conductivity, alternating directions (with $g = g_2$).

Impediography

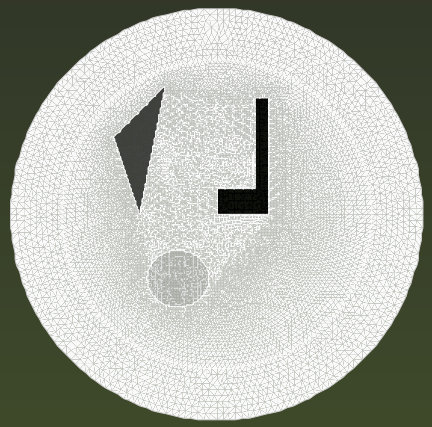

(a) True conductivity

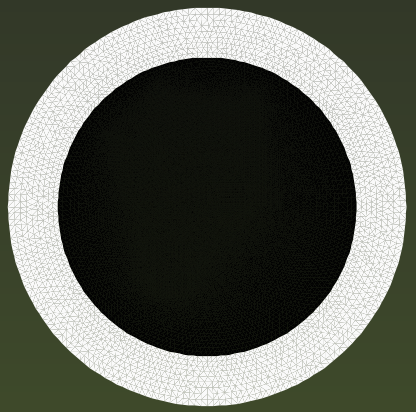

(b) Initial guess

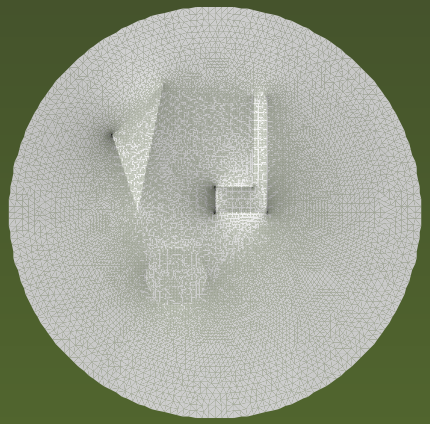

(c) Measurements

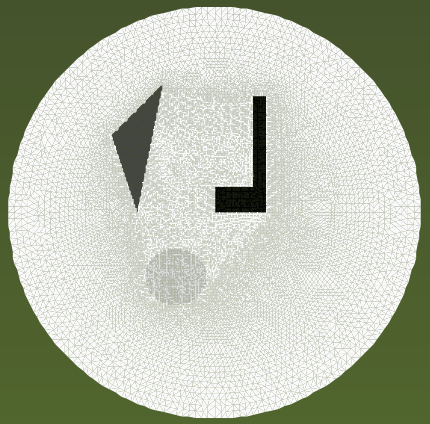

(d) Reconstructed map

Vibration Potential Tomography: Physical Background

- (with Y. Capdeboscq, H. Kang, and A. Kozhemyak, EJAP 09)
- Ultrasonic waves are focused on regions of small diameter inside a charged body placed on a static magnetic field.
- Compared to Impediography: Instead of creating a perturbation in the conductivity, create a source term using Lorenz force density which is proportional to the local electrical conductivity.

Vibration Potential Tomography

- Replace the conductivity problem by a Nonlinear PDE:

$$\begin{cases} \nabla \cdot \left(\dfrac{\mathcal{E}}{u} \nabla u \right) = 0 & \text{in } \Omega \ , \\ u = f & \text{on } \partial\Omega \ . \end{cases}$$

  Reconstruct γ from

$$\mathcal{E}(z)/u(z) = \gamma(z), \quad z \in \Omega.$$

- $\mathcal{E}$ computed from the boundary measurements.

Vibration Potential Tomography: Reconstruction

A simple minded solution: put $w = \ln u$, then w is the solution to

$$\begin{cases} \nabla \cdot \mathcal{E} \nabla w = 0 & \text{in } \Omega, \\ w = \ln f & \text{on } \partial\Omega, \end{cases}$$

Then $\gamma(z) = \dfrac{\mathcal{E}(z)}{\exp w(z)}$. (Error may be amplified.)

Vibration Potential Tomography: Numerical Example

Linearization Procedure:

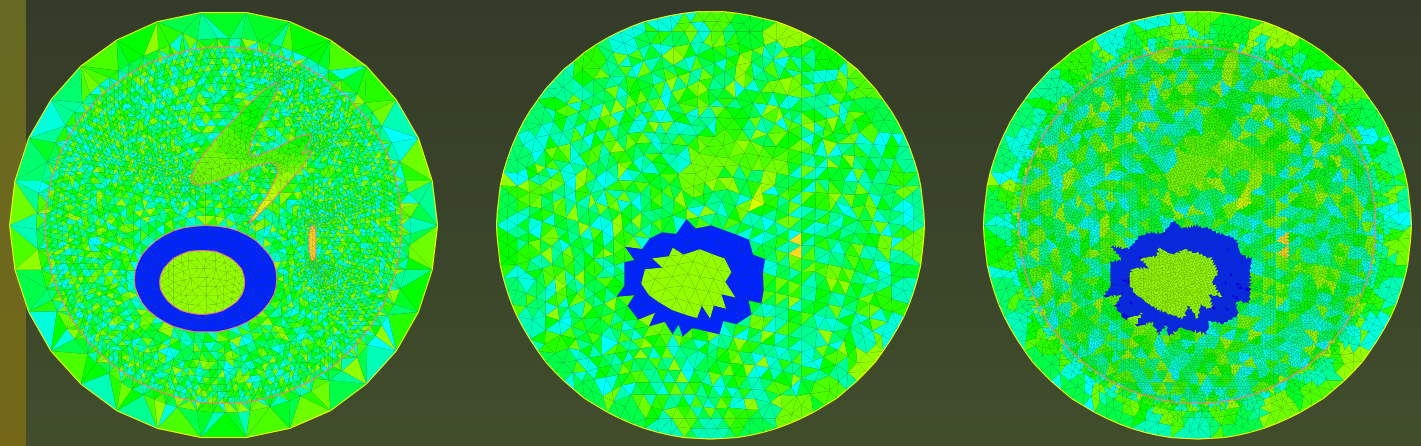

Figure 3: Left: actual conductivity distribution; middle: conductivity projected onto pixels; right: reconstructed conductivity

Vibration Potential Tomography: Numerical Example

Optimal Control Approach:

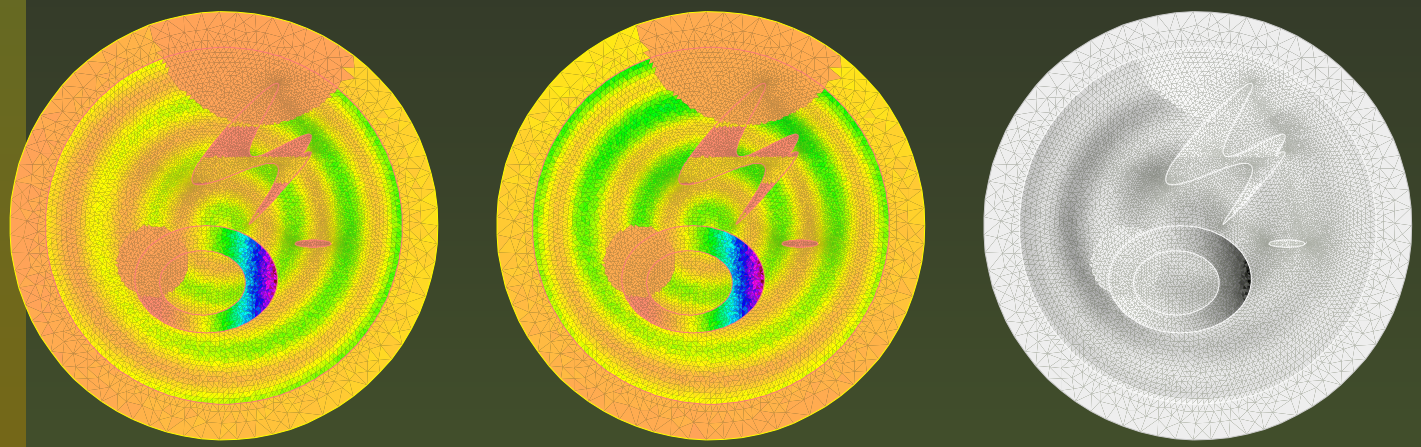

Figure 4: Perturbed reconstruction test with incomplete data.

Magnetic Resonance Elastography

- (with P. Garapon, H. Kang, and H. Lee, Quart. Appl. Math. 08)
- Initial idea: the shear elasticity can be correlated with the pathological state of tissues.
- Detect the shape, the location, and the shear modulus of an elastic anomaly from internal measurements of the displacement field generated by an external vibration.
- Compressional modulus is 4 orders of magnitude larger than the shear modulus in biological tissues (quasi-incompressibility).

Magnetic Resonance Elastography

- Formula $\mu = -\omega^2 \rho u / \Delta u$ is not a right approximation.
- Assumption of incompressibility ($\nabla \cdot u = 0$) is not correct.
- Taking derivatives amplifies the error (in particular across the boundary of the anomaly).

Magnetic Resonance Elastography

- The elasticity system should be replaced by a modified Stokes system.
- The elastic moment tensor $M(B, \lambda, \mu, \tilde{\lambda}, \tilde{\mu})$ (B scaled domain) characterizes all the information about an elastic anomaly that can be learned from boundary measurements.
- P: orthogonal projection from the space of symmetric matrices onto the space of symmetric matrices with trace zero

$$PM(B, \lambda, \mu, \tilde{\lambda}, \tilde{\mu})P \text{ has a limit as } \lambda, \tilde{\lambda} \to +\infty.$$

- Notion of a Viscous Moment Tensor as the limit of PMP, M: the elastic moment tensor.

Magnetic Resonance Elastography

- Similar inner and outer expansions as the ones for the scalar problem hold.
- Local algorithm for reconstructing the shape and the shear modulus of the anomaly from the inner expansion is developed.
- (with P. Gapaon and F. Jouve, JCM 09) Satisfactory results obtained from minimizing the discrepancy functional in the near-field of the anomaly.
- Minimization of the discrepancy functional: trade of between resolution and stability.
- Quantify the window size.

Magnetic Resonance Elastography

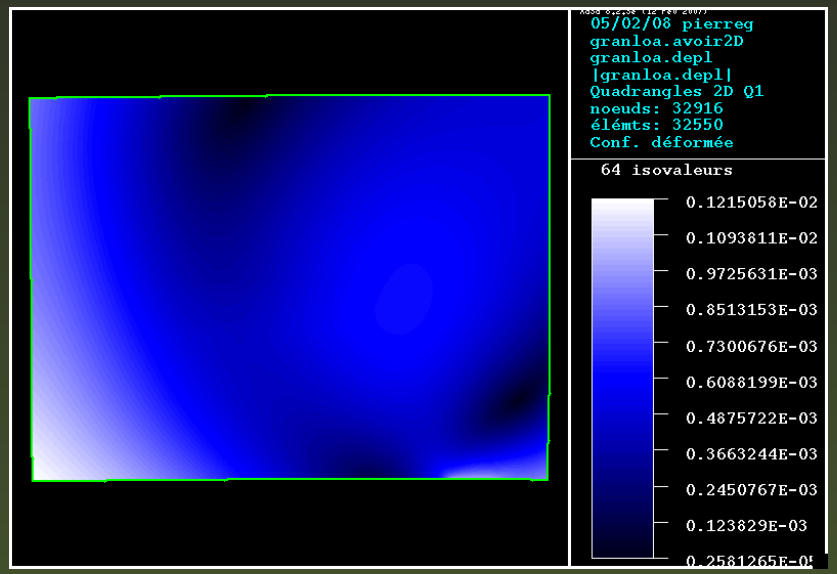

Figure 5: Internal displacement field

Magnetic Resonance Elastography

Figure 6: Reconstruction from internal elastic measurements

Magnetic Resonance Elastography

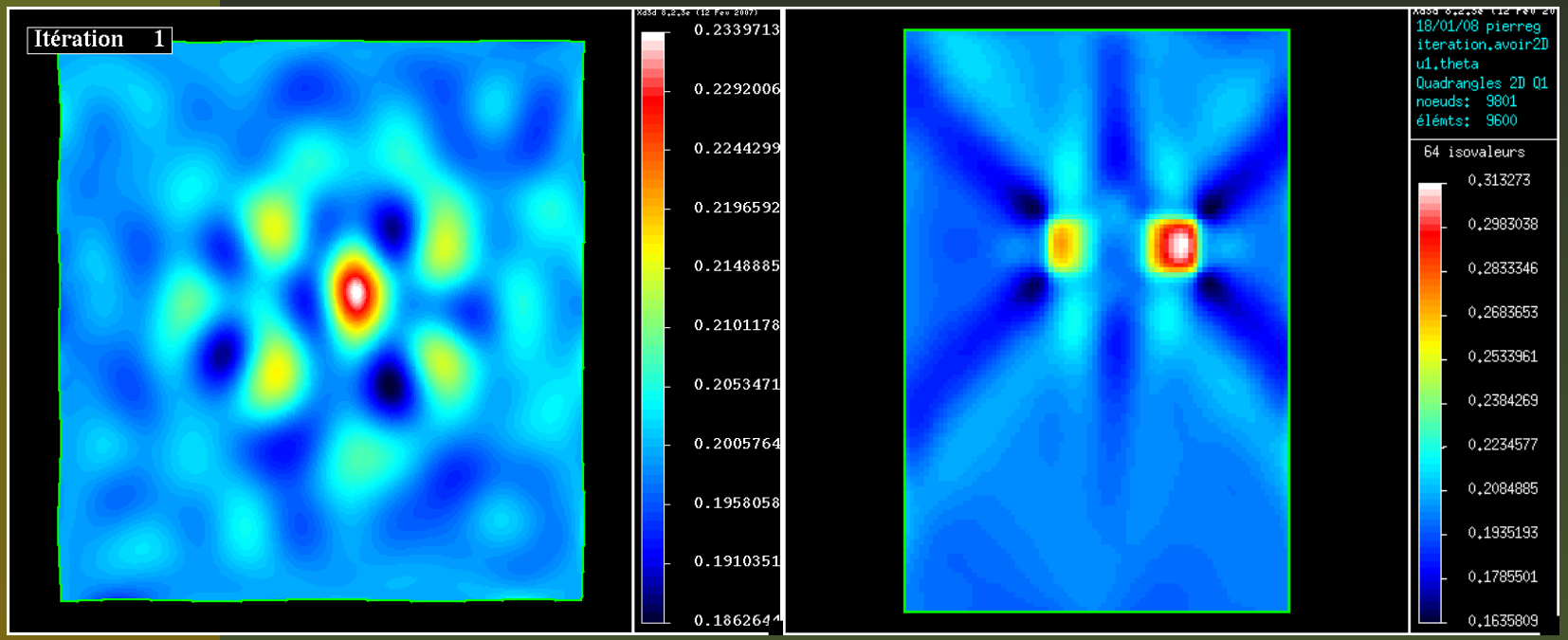

Figure 7: Achievable resolutions

Photo-Acoustic Imaging

- (with E. Bossy, V. Jugnon, and H. Kang, SIAM Rev. 09)
- Photo-acoustic imaging: generation of acoustic waves by the absorption of optical energy. Reconstruct absorbing regions inside the organ from boundary measurements of the induced acoustic signal.
- D_l: absorbing regions inside the organ
- A_l: absorbed optical energy density in D_l.
- A_l: absorbed optical energy density in D_l.
- $A_l = \mu_l \Phi$, μ_l: optical absorption coefficient, Φ: light fluence.

Photo-Acoustic Imaging

$$\frac{\partial^2 p}{\partial t^2}(x,t) - c_s^2 \Delta p(x,t) = 0, \quad x \in \Omega, \quad t \in]0,T[,$$

c_s: acoustic speed in Ω.

Initial conditions

$$p|_{t=0} = \sum_{l=1}^{m} \chi_{D_l}(x) A_l(x) \quad \text{and} \quad \left.\frac{\partial p}{\partial t}\right|_{t=0} = 0 \quad \text{in } \Omega.$$

Boundary conditions:

$$p = 0 \quad \text{or} \quad \frac{\partial p}{\partial \nu} = 0 \quad \text{on } \partial\Omega \times]0,T[.$$

Photo-Acoustic Imaging

- Without boundary conditions: Spherical Radon transform

$$p(x,t) = \frac{c_s}{4\pi}\frac{d}{dt}\left[t\sum_{l=1}^{m}\int_{|x'|=1}\chi_{D_l}(x+c_s t x')A_l(x+c_s t x')\,dS(x')\right].$$

- P. Kuchment, O. Scherzer
- With boundary conditions, spherical Radon transform does not apply.

Photo-Acoustic Imaging

- For $y \in \mathbb{R}^3 \setminus \overline{\Omega}$,

$$v_y(x,t;\tau) := \frac{\delta\left(t+\tau-\frac{|x-y|}{c_s}\right)}{4\pi|x-y|} \quad \text{in } \Omega\times]0,T[,$$

$\tau > \frac{\text{dist}(y,\partial\Omega)}{c_s}$: a parameter.

- Use $\tau \mapsto \int_0^T \int_{\partial\Omega} \frac{\partial p}{\partial \nu}(x,t) v_y(x,t;\tau)\, d\sigma(x)\, dt$: probe the medium as a function of τ.

Photo-Acoustic Imaging

- The probe is nonzero only on the interval $]\tau_a, \tau_e[$, τ_a: arrival-time, τ_e: exit-time of the sphere of center y and radius τ hits D.
- Convolution of the data with an incoming wave $\Rightarrow$ strong connection with time-reversal techniques.
- Reconstruct the optical absorbtion coefficient μ inside the small absorbing region from the absorbed optical energy density. ($A = \mu\Phi$, Φ solution to the diffusion Eq.).

Photo-Acoustic Imaging

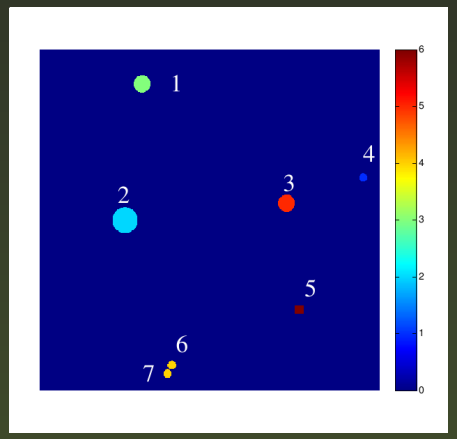

(a) Real configuration of the medium.

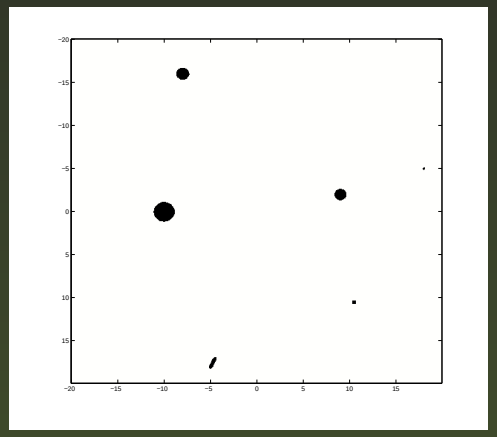

(b) Reconstructed image of the medium.

Figure 8: Real and reconstructed configurations of the medium.

Photo-Acoustic Imaging: Selective Imaging

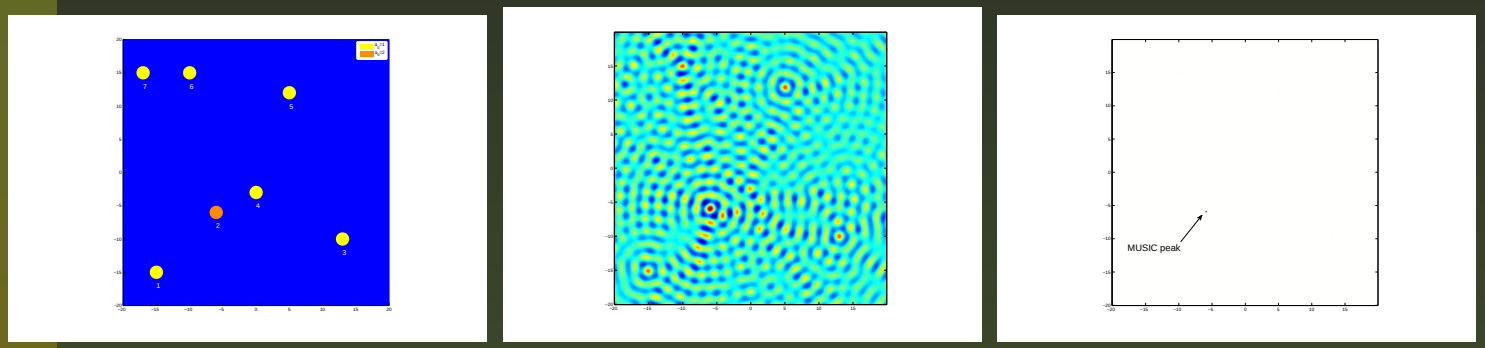

Figure 9: MUSIC simulation with 7 inclusions, contrast=2.

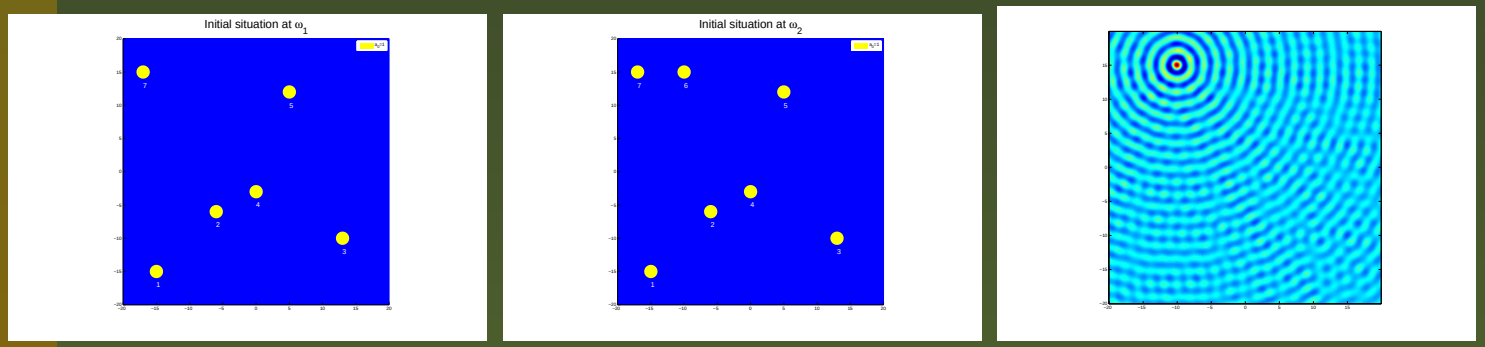

Figure 10: Multi-frequency approach results.

Conclusion

- Promising:
  - Multi-Scale + Multi-Physics imaging approaches
- Important:
  - Develop Boundary independent imaging/Multi-frequency imaging
  - Control the trade-off between Resolution/Stability